

On the retrieval of ice cloud particle shapes from POLDER measurements

Wenbo Sun^{a,*}, Norman G. Loeb^a, Ping Yang^b

^aCenter for Atmospheric Sciences, Hampton University, Hampton, VA 23668, USA

^bDepartment of Atmospheric Sciences, Texas A & M University, College Station, TX 77843, USA

Abstract

Shapes of ice crystals can significantly affect the radiative transfer in ice clouds. The angular distribution of the polarized reflectance over ice clouds strongly depends on ice crystal shapes. Although the angular-distribution features of the total or polarized reflectance over ice clouds imply a possibility of retrieving ice cloud particle shapes by use of remote sensing data, the accuracy of the retrieval must be evaluated. In this study, a technique that applies single ice crystal habit and multidirectional polarized radiance to retrieve ice cloud particle shapes is assessed. Our sensitivity studies show that the retrieved particle shapes from this algorithm can be considered good approximations to those in actual clouds in calculation of the phase matrix elements. However, this algorithm can only work well under the following conditions: (1) the retrievable must be overcast and thick ice cloud pixels, (2) the particles in the cloud must be randomly oriented, (3) the particle shapes and size distributions used in the lookup tables must be representative, and (4) the multi-angle polarized measurements must be accurate and sufficient to identify ice cloud pixels of randomly oriented particles. In practice, these conditions will exclude most of the measured cloud pixels. Additionally, because the polarized measurements are only sensitive to the upper cloud part not deeper than an optical thickness of 4, the retrieved particle shapes with the polarized radiance may only approximate those in the upper parts of the clouds. In other words, for thicker clouds with vertical inhomogeneity in particle shapes, these retrieved particle shapes cannot represent those of whole clouds. More robust algorithm is needed in accurate retrieval of ice cloud particle shapes.

© 2006 Elsevier Ltd. All rights reserved.

Keywords: Retrieval; Ice cloud; Particle shape; POLDER

1. Introduction

Cirrus clouds, primarily present in the upper troposphere and lower stratosphere, are globally distributed and composed almost exclusively of nonspherical ice crystals [1]. Shapes of ice crystals can significantly affect the radiative transfer in ice clouds. The angular distribution of the upward radiances over ice clouds also depends on the ice crystal shapes. Retrievals of actual cirrus particle shapes from satellite-measured radiances are highly difficult because of the extremely large variability in ice crystal sizes and habits [2]. The variability of ice crystal

*Corresponding author. NASA Langley Research Center, Mail Stop 420, Hampton, VA 23681-0001, USA. Tel.: +1 757 864 9986; fax: +1 757 864 7996.

E-mail address: w.sun@larc.nasa.gov (W. Sun).

sizes and shapes could affect the angular distributions of the total radiances over ice clouds. This makes it possible to use satellite-measured radiances at different viewing angles to retrieve particle shapes [3]. However, because of multiple scattering in clouds, radiances at different viewing angles are not determined solely by particle shapes. The particle size distribution and the optical thickness of the cloud also play important roles in the angular distribution of the upward radiances. Therefore, ambiguities could hardly be avoided in the retrieval of particle shapes using total radiances at two or even more viewing angles. Another approach is to use the multidirectional polarized radiances from the POLARization and Directionality of the Earth Reflectance (POLDER) [4] to retrieve the particle shapes in ice clouds [5]. The polarized radiances are highly sensitive to particle shapes and independent of optical thickness when optical thickness is larger than 4 [5,6]. The particle shape retrieval algorithm based on the polarized measurements can somewhat remove the ambiguities caused by the uncertainty of optical thickness, but its accuracy is also strongly determined by the assumed model particle shapes. Using highly simplified particle shapes such as hexagonal crystals with different aspect ratios [5,6] in the retrieval algorithm may not be able to produce a reliable picture for actual particle shapes in ice clouds.

In this study, to evaluate the technique which applies single ice crystal habit and multidirectional polarized radiance to retrieve ice cloud particle shapes, a multidirectional polarized reflectance matching (MPRM) algorithm is developed for the retrieval of ice cloud particle shapes using POLDER polarized measurement at 865 nm. In Section 2, the POLDER polarized measurements are introduced. In Section 3, the MPRM algorithm is developed for the retrieval of ice cloud particle shapes using the POLDER polarized measurements. In Section 4, a theoretical sensitivity study on the accuracy of the ice cloud particle shape retrieval is presented and the retrieval results from 5-month POLDER data are analyzed. Conclusions are given in Section 5.

2. POLDER polarized data

The POLDER instrument [4] is based on a two-dimensional charged coupled device (CCD) detector array, a rotating wheel carrying spectral and polarized filters, and wide field of view optics. It is designed to measure normalized total and polarized radiances at the top of the atmosphere (TOA). The POLDER-I onboard ADEOS-1 performed measurements for 8 months, from November 1, 1996 to June 30, 1997. On a sun-synchronous orbit with an altitude of 797 km, POLDER-I has a swath width of ~2200 km and a pixel size of ~6 km × 7 km at nadir. As the ADEOS satellite passes over a scene, up to 14 successive measurements are acquired from various viewing geometries in eight narrow spectral bands between 443 and 910 nm. The polarized radiance at the top of atmosphere is measured in three different channels: 443, 670, and 865 nm. The accuracy of the normalized polarized radiance is 0.001 [5]. The “ERB, water vapor and clouds” processing line results [7] in the POLDER-I level 2 products are averaged over 9 × 9 original POLDER pixels, resulting in “super-pixels” with a spatial resolution of ~60 km × 60 km. This processing line provides cloud parameters such as cloud fraction and cloud phase, as well as solar and viewing geometries. Cloud fraction is determined by applying a cloud detection algorithm to each full-resolution pixel and viewing direction [8]. Cloud phase is determined using the differences in polarized reflectance at 865 nm between liquid water and ice clouds in different scattering angle ranges [9]. In this study, the multiple-angular polarized radiance measurements at 865 nm from overcast ice cloud super-pixels over ocean in POLDER-I level 2 dataset are used to examine the particle shapes in ice clouds.

3. Multidirectional polarized reflectance matching algorithm

3.1. Method

Given the Stokes parameters of the emergent light at TOA, i.e. (I , Q , U , V), one can calculate the polarized reflectance at a given wavelength as [5]

$$R = \frac{\pi \sqrt{Q^2 + U^2 + V^2}}{E_s \cos \theta_0}, \quad (1)$$

where E_s denotes the incident solar flux at the given wavelength and θ_0 is the solar zenith angle.

Using a database of theoretical TOA polarized reflectance at 865 nm for various combinations of particle shapes and size distributions, the MPRM method searches the database to find the cloud model (as a function of particle shape and size distribution) that provides the best match to multi-angle POLDER polarized data over each super-pixel. For a set of instantaneous POLDER multidirectional measurements, we search through the database for the cloud model that provides the minimum value of the following parameter:

$$s^2(\theta_0, p) = \sum_{n=1}^{N_d} [R_m(\theta_0, \theta_n, \varphi_n) - R_t(\theta_0, \theta_n, \varphi_n, p)]^2, \quad (2)$$

where R_m and R_t are the measured and theoretical polarized reflectance, respectively; N_d is the number of the POLDER measurements used in the retrieval, θ_n and φ_n are the viewing zenith and azimuth angles for a given viewing geometry, and p denotes the scattering phase matrix determined by ice crystal shape and size distribution at the measurement wavelength. The particle shape corresponding to the minimum $s^2(\theta_0, p)$ is the retrieved ice crystal habit of the measured pixel.

3.2. Ice cloud model

We assume a single layer of plane-parallel cloud composed of ice crystals in the height range of 8–9 km over ocean. Because the polarized radiances are independent of optical thickness when optical thickness is larger than 4 [5,6], the optical thickness of the cloud is assumed to be 5 so that the lookup tables (LUTs) based on this cloud model are independent of optical thickness. In this study, we employ eight particle shapes for the assumed ice cloud layer, i.e. solid hexagonal columns, hollow hexagonal columns, plates, bullet rosettes, 6-branch bullet rosettes, aggregates, rough-surfaced bullet rosettes, and rough-surfaced aggregates. The shapes for solid hexagonal columns, hollow hexagonal columns, plates, bullet rosettes, 6-branch bullet rosettes, and aggregates are illustrated in Fig. 1. Rough-surfaced bullet rosettes and rough-surfaced aggregates can be described as the corresponding shapes in Fig. 1 with roughness on their surfaces. Based on measurements [2], these ice crystal habits are more realistic than those used in [5,6]. The single-scattering properties of these ice crystals are calculated using a light-scattering computational code described in Yang et al. [10]. To provide a reliable retrieval of the particle shapes in ice clouds, a wide range of observed ice crystal size distributions is needed. In calculation of the volume-averaged single-scattering properties of the ice clouds, 28 ice crystal size distributions based on in situ aircraft observations of both midlatitude and tropical ice clouds [11] and two average ice crystal size distributions from the First International ISCCP Regional Experiment (FIRE) [12] are employed. These size distributions are significantly different and our calculations show that their effects on volume-averaged single-scattering properties of ice clouds are not trivial. Therefore, we have 240 different ice cloud models from combinations of particle shapes and size distributions.

3.3. Lookup table

LUTs of TOA polarized reflectance at 865 nm are constructed using the adding-doubling radiative transfer program [13]. Because of the weak gas absorption at 865 nm, only Rayleigh scattering is included in the atmosphere. The surface is assumed to be black since the ocean contribution to the measured polarized reflectance is weak when the pixel is overcast by thick cloud. For different solar zenith angles, we produce LUTs of ice cloud polarized reflectance as function of viewing zenith angle θ , relative azimuth angle φ , and cloud model index. For the LUTs, the solar zenith angle, viewing zenith angle, and relative azimuth angle range from 0° to 75° , 0° to 75° , and 0° to 180° , respectively, with an increment of 3° . Fig. 2 shows a comparison of the TOA polarized reflectance at 865 nm from ice clouds composed of solid hexagonal columns, hollow hexagonal columns, plates, bullet rosettes, 6-branch bullet rosettes, rough-surfaced bullet rosettes, aggregates, and rough-surfaced aggregates, respectively. The ice crystal size distribution in the cloud layer is determined from the parameterization by Heymsfield and Platt [14] for a temperature range of -20 to -25°C . The TOA polarized reflectance in Fig. 2 is from a LUT with a solar zenith angle of 60° . We can see that the angular distributions of polarized reflectance at TOA are strongly dependent on the particle shape. Solid columns produce the most significant polarized reflectance variations with viewing angles. The magnitude of the

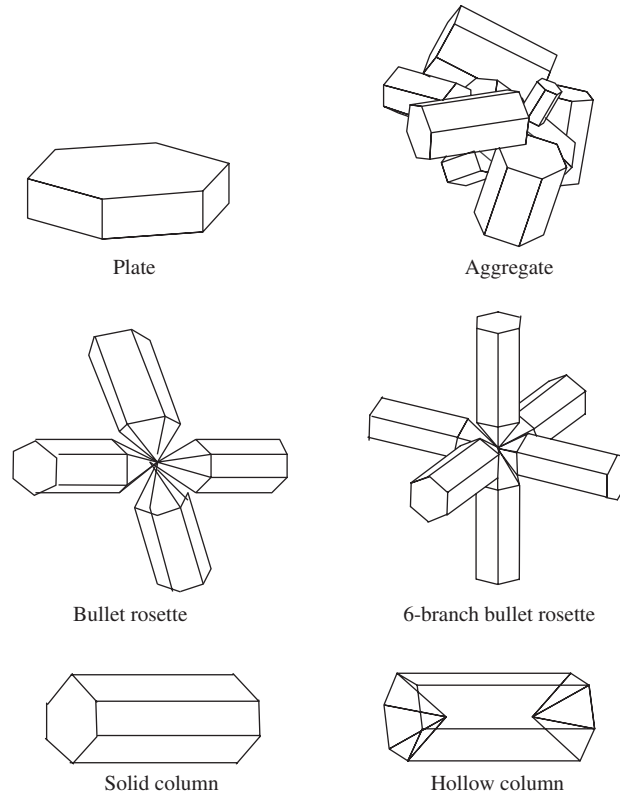


Fig. 1. Shapes for solid hexagonal columns, hollow hexagonal columns, plates, bullet rosettes, 6-branch bullet rosettes, and aggregates.

polarized reflectance from plates is the biggest but still smaller than 0.08. The polarized reflectance of ice clouds is relatively small.

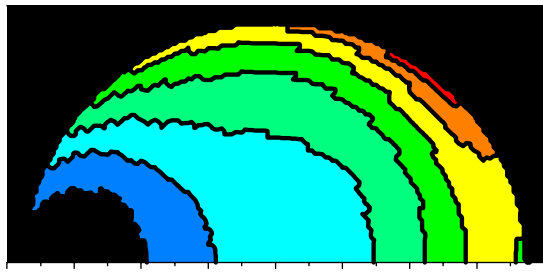
4. Results

4.1. Sensitivity study

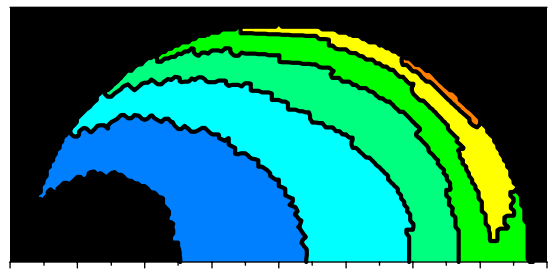
To test the MPRM algorithm, polarized reflectances from adding-doubling radiative transfer program for a layer of hypothetical ice cloud are used as input to the MPRM algorithm at the POLDER super-pixel solar and viewing geometries during December 1–31, 1996. To ensure the accuracy of the algorithm, the retrievals throughout this study are performed only for super-pixels with more than 4 angular measurements. Actually, most super-pixels in POLDER data have more than 4 angular measurements. Super-pixels within a latitude range of 60°S to 60°N and with solar zenith angles smaller than 75° are analyzed. The accuracy of the reflectance matching is determined from the relative matching error (RME) as

$$\text{RME} = \frac{\sqrt{1/N_d \sum_{n=1}^{N_d} [R_m(\theta_0, \theta_n, \varphi_n) - R_t(\theta_0, \theta_n, \varphi_n, P_{rtw})]^2}}{1/N_d \sum_{n=1}^{N_d} R_m(\theta_0, \theta_n, \varphi_n)} \times 100\%, \quad (3)$$

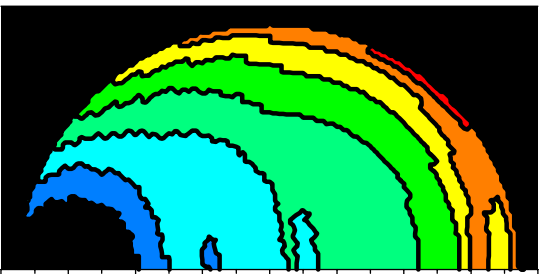
Fig. 2. Model-simulated TOA polarized reflectance at 865 nm as function of viewing zenith angle (0–75° in radial direction from origin “O”) and relative azimuth angle (0–180° in anticlockwise direction around origin “O”) from ice clouds composed of (a) aggregates, (b) rough-surfaced aggregates, (c) 6-branch bullet rosettes, (d) bullet rosettes, (e) rough-surfaced bullet rosettes, (f) hollow columns, (g) plates, and (h) solid columns. The ice crystal size distribution in the cloud layer is determined from the parameterization by Heymsfield and Platt [14] for a temperature range of –20 to –25 °C. A solar zenith angle of 60° is used.



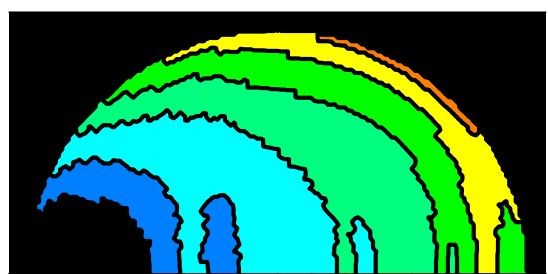
(a) 0 0.0038 0.0075 0.011 0.015 0.019 0.023 0.026 0.030



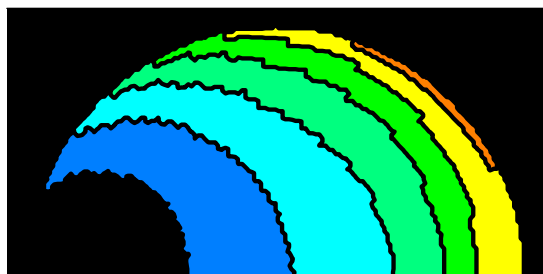
(b) 0 0.0044 0.0087 0.013 0.017 0.022 0.026 0.031 0.035



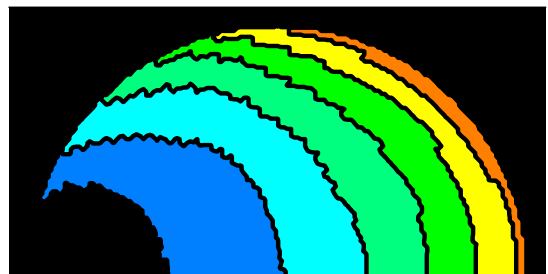
(c) 0 0.0044 0.0087 0.013 0.017 0.022 0.026 0.031 0.035



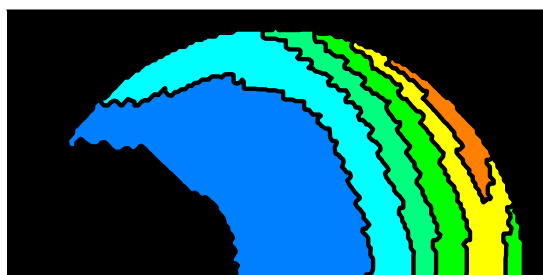
(d) 0 0.0050 0.010 0.015 0.020 0.025 0.030 0.035 0.040



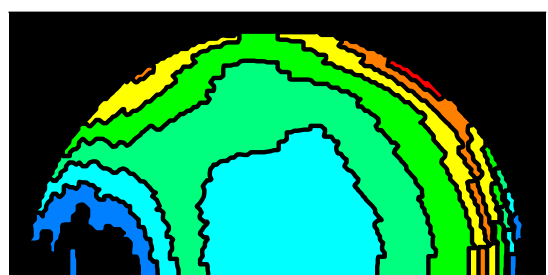
(e) 0 0.0044 0.0087 0.013 0.017 0.022 0.026 0.031 0.035



(f) 0 0.0056 0.011 0.017 0.022 0.028 0.034 0.039 0.045



(g) 0 0.010 0.020 0.030 0.040 0.050 0.060 0.070 0.080
TOA polarized reflectance at 865 nm



(h) 0 0.0044 0.0087 0.013 0.017 0.022 0.026 0.031 0.035
TOA polarized reflectance at 865 nm

where p_{riv} denotes the scattering phase matrix determined by the retrieved ice crystal shape and size distribution at the measurement wavelength. As a zero-order test, the retrieval algorithm was firstly applied to hypothetical clouds consisted of single particle shapes. The results show that the algorithm can exactly find the correct single shapes as the retrieved, because without error perturbation in the hypothetical reflectance data, the multi-angle polarized reflectance feature of cloud of single particle shape is unique, as shown in Fig. 2. To validate the algorithm for natural ice clouds composed of various particle shapes, we must test the algorithm on a more complicated hypothetical ice cloud model. We assume that the hypothetical ice cloud is confined to a layer between 8 and 9 km with an optical thickness of 5. The ice cloud layer is assumed to be composed of a mixture of hexagonal plates, hollow hexagonal columns, bullet rosettes, and aggregates. Based on the habit percentage data from the first ISCCP regional experiment (FIRE II) intensive field observation (IFO), the following method to model the habit combinations is chosen [15,16]: When the maximum dimension of the ice crystal is smaller than $70\ \mu\text{m}$, the ice crystal within the size region is assumed to be composed of 50% bullet rosettes, 25% hexagonal plates, and 25% hollow hexagonal columns; when the maximum dimension of the ice crystal is larger than $70\ \mu\text{m}$, the ice crystal within the size region is assumed to be composed of 30% aggregates, 30% bullet rosettes, 20% hexagonal plates, and 20% hollow hexagonal columns. The ice crystal size distribution in the cloud layer is determined from the parameterization by Heymsfield and Platt [14] for a temperature range of -20 to $-25\ ^\circ\text{C}$.

Fig. 3(a) shows the RME distribution for the hypothetical ice cloud with an optical thickness of 5. The RME remains less than 10% for most cases. Because the absolute value of the polarized reflectance is relatively small, the RME for this study actually is not large, which means the polarized reflectance from combined particle shapes matches that from the single particle habits quite well.

Figs. 3(b) shows the super-pixel numbers as function of the particle shapes retrieved from the hypothetical ice cloud. We can see that for the layer of ice cloud composed of the given combined ice crystal habits, the retrieved particle shapes are dominated by bullet rosettes and hollow hexagonal columns. At scattering angles larger than $\sim 40^\circ$, the two particle shapes both have medium scattering features compared to strong-featured hexagonal plates and relatively featureless aggregates. Although in the mixture of ice crystal habits significant ratios of aggregates and hexagonal plates are included, the retrieved shapes show little relation to the two shapes. Because the retrieval is performed on the cloud with averaged single-scattering properties of different particle shapes, the MPRM algorithm searches the averaged scattering features in the LUTs and takes the best match as the retrieved. Depending on the incidence and viewing geometries, the averaged scattering features of the same cloud vary with the measurement angles. Therefore, as shown in Fig. 3(b), the retrieved particle shapes of the same cloud based on single-habit cloud models are not identical, but show a distribution of different habits. We can see in Fig. 4 that all of the nonzero scattering phase matrix elements of the 6-branch bullet rosettes, bullet rosettes, and hollow hexagonal columns are quite close to those of the mixture of particle shapes in the hypothetical ice cloud. Additionally, Figs. 5 and 6 show that the phase matrix elements of mixture of particle shapes in the hypothetical ice cloud are significantly different from those of hexagonal plates, aggregates, rough aggregate, solid hexagonal columns, and rough bullet rosettes. Therefore, the result shown in Fig. 3(b) does not include these particle shapes. Because the three retrieved particle shapes result in similar scattering properties as shown in Fig. 4, the uncertainty in these particle shapes will not cause significant errors in radiative transfer in clouds composed of these particles.

4.2. A look from 5-month POLDER data

The MPRM particle shape retrieval algorithm is applied to 5-month POLDER data measured in November and December 1996, and April, May, and June 1997 for a latitude range of 60°S to 60°N and solar zenith angles smaller than 75° . In this retrieval, only overcast super-pixels with ice cloud optical thickness larger than 4 are considered because the LUTs are made simply for thick ice clouds. To select clouds formed only by randomly oriented particles, we check the polarized reflectance peak within a glint angle of 5° . If there is a peak of polarized reflectance at this reflection angle range, the particles in the measured super-pixel are not randomly oriented [5]. Therefore, two additional actions are performed on the data: (1) super-pixels without a measurement within a glint angle (the angle between reflected ray and specular ray) of 5° are excluded; (2) if there is a measured polarized reflectance $R_m(\theta_0, \theta_n, \varphi_n)$ within a glint angle of 5° , but

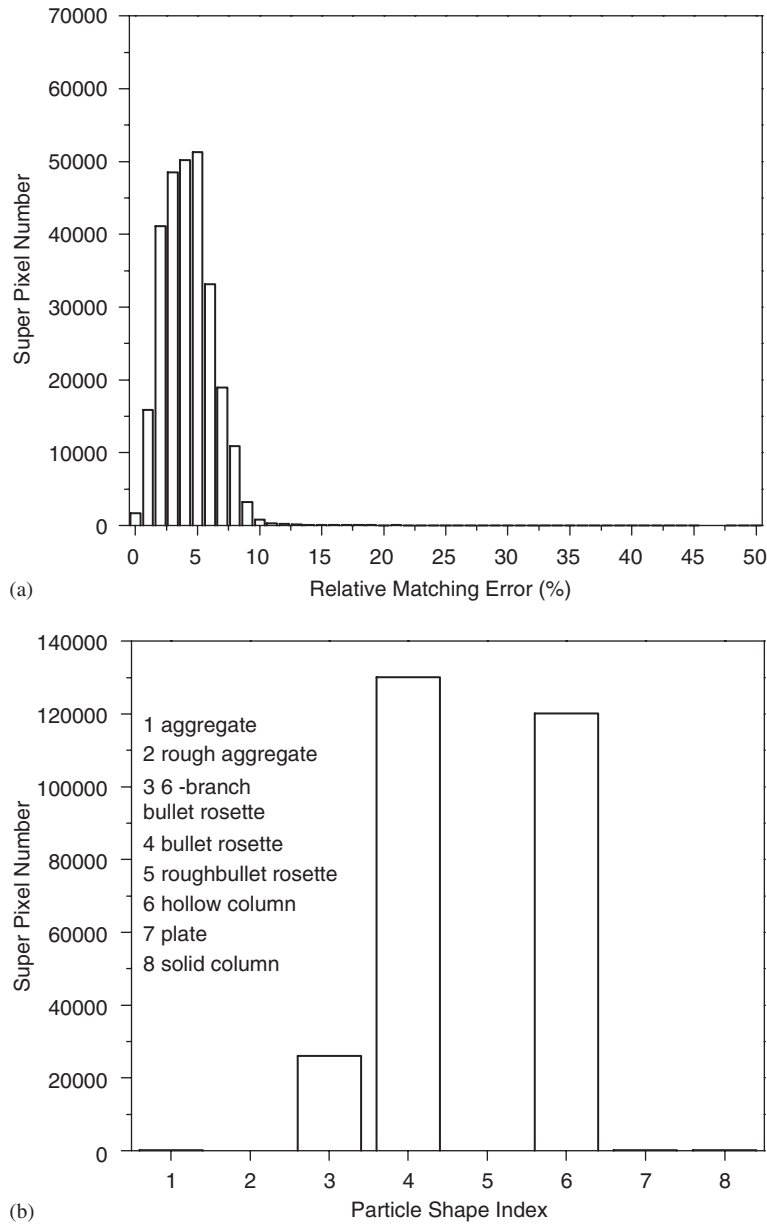


Fig. 3. (a) Relative matching error (RME) distribution for the hypothetical ice cloud with an optical thickness of 5. (b) Super-pixel numbers as function of the particle shapes retrieved from the hypothetical ice cloud. The POLDER super-pixel solar and viewing geometries during December 1–31, 1996 are used, which correspond to 276473 super-pixels.

$R_m(\theta_0, \theta_n, \varphi_n) - R_m(\theta_0, \theta_{n-1}, \varphi_{n-1}) > 0.001$ and $R_m(\theta_0, \theta_n, \varphi_n) - R_m(\theta_0, \theta_{n+1}, \varphi_{n+1}) > 0.001$, the super-pixel is excluded. Since there is very small chance the POLDER instrument can actually measure the radiance at the specular reflection angle, filtering the data for super-pixels of randomly oriented particles using the neighboring measurements around the specular reflection angle will exclude most of the available data. Our test shows that only 0.31% of the super-pixels in the 5-month POLDER data can pass the pixel selection criteria.

Fig. 7(a) shows the RME distribution for ice cloud super-pixels observed in November and December 1996, and April, May, and June 1997 between latitude 60°S and 60°N with solar zenith angles smaller than 75°. The RME in Fig. 7(a) is larger than that in Fig. 2(a) because many factors in the actual clouds are different from

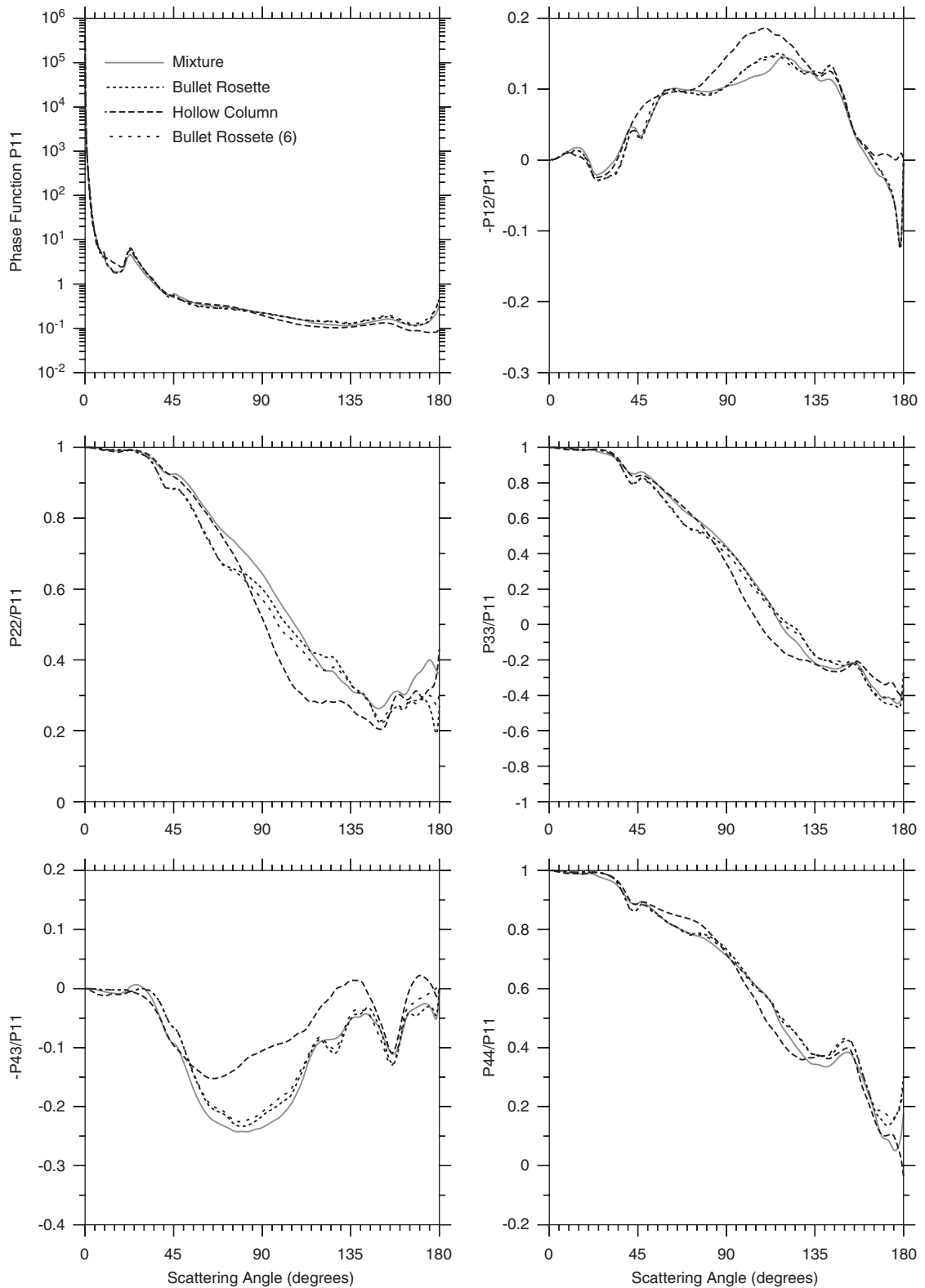


Fig. 4. Scattering phase matrix elements of the mixture of different particle shapes of the hypothetical cloud and those of bullet rosettes and hollow hexagonal columns at a wavelength of 865 nm. The ice crystal size distribution in the clouds is determined from the parameterization by Heymsfield and Platt [14] for a temperature range of -20 to -25 °C. In this figure, Bullet Rosette (6) denotes 6-branch bullet rosettes.

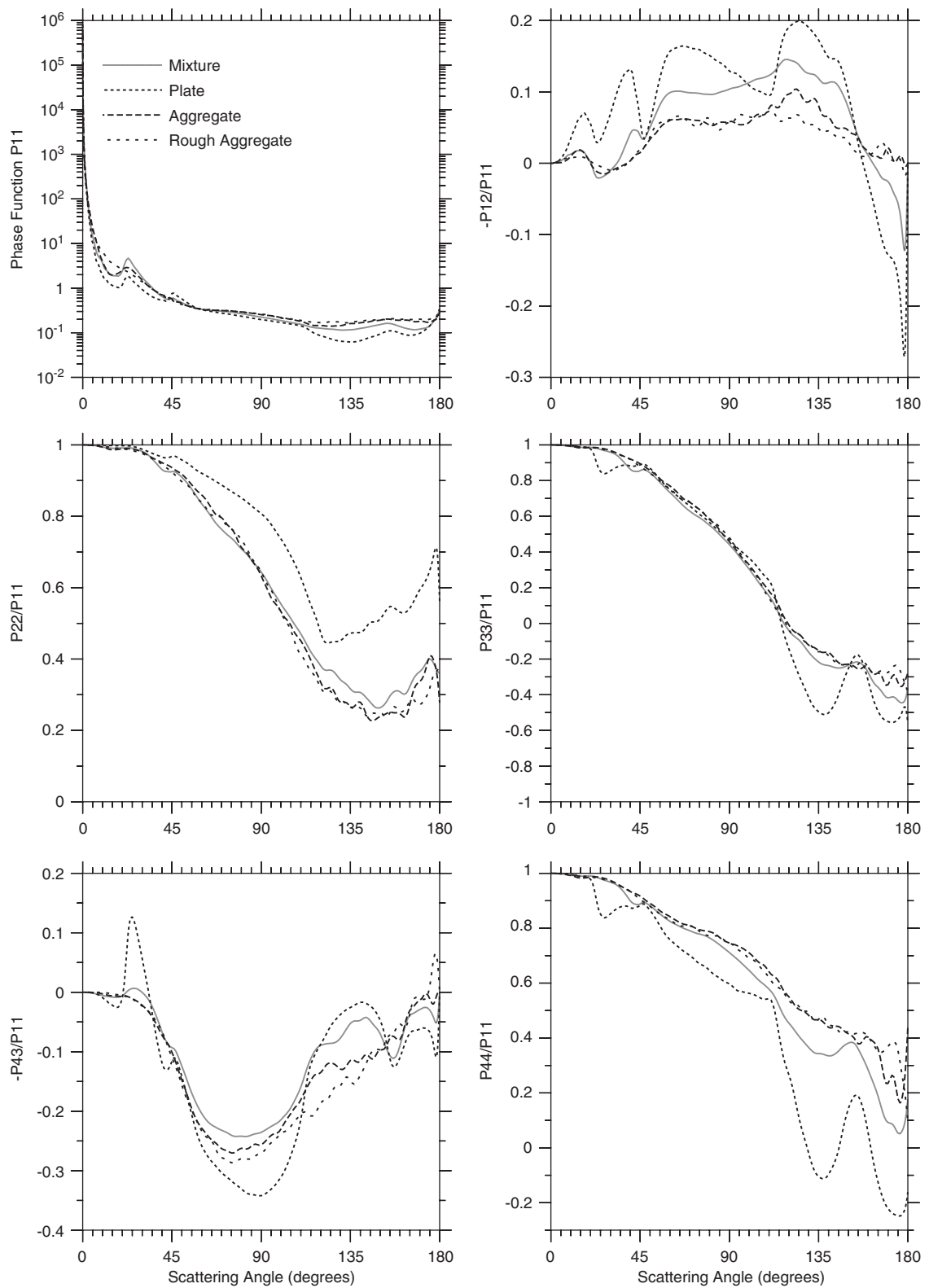


Fig. 5. Same as Fig. 4, but for scattering phase matrix elements of the mixture of different particle shapes and those of plates, aggregates, and rough-surfaced aggregates.

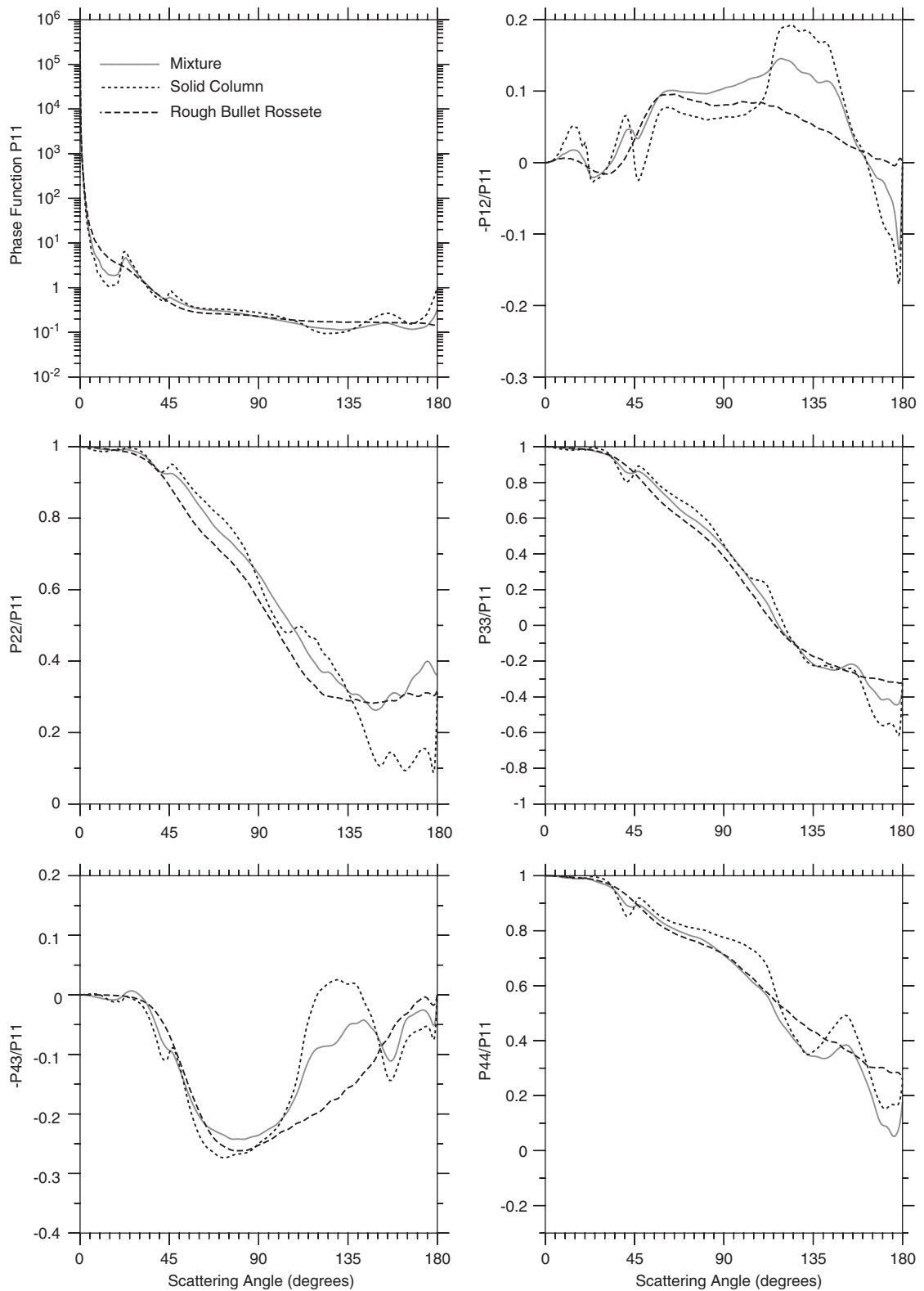


Fig. 6. Same as Fig. 4, but for scattering phase matrix elements of the mixture of different particle shapes and those of solid hexagonal columns and rough-surfaced bullet rosettes.

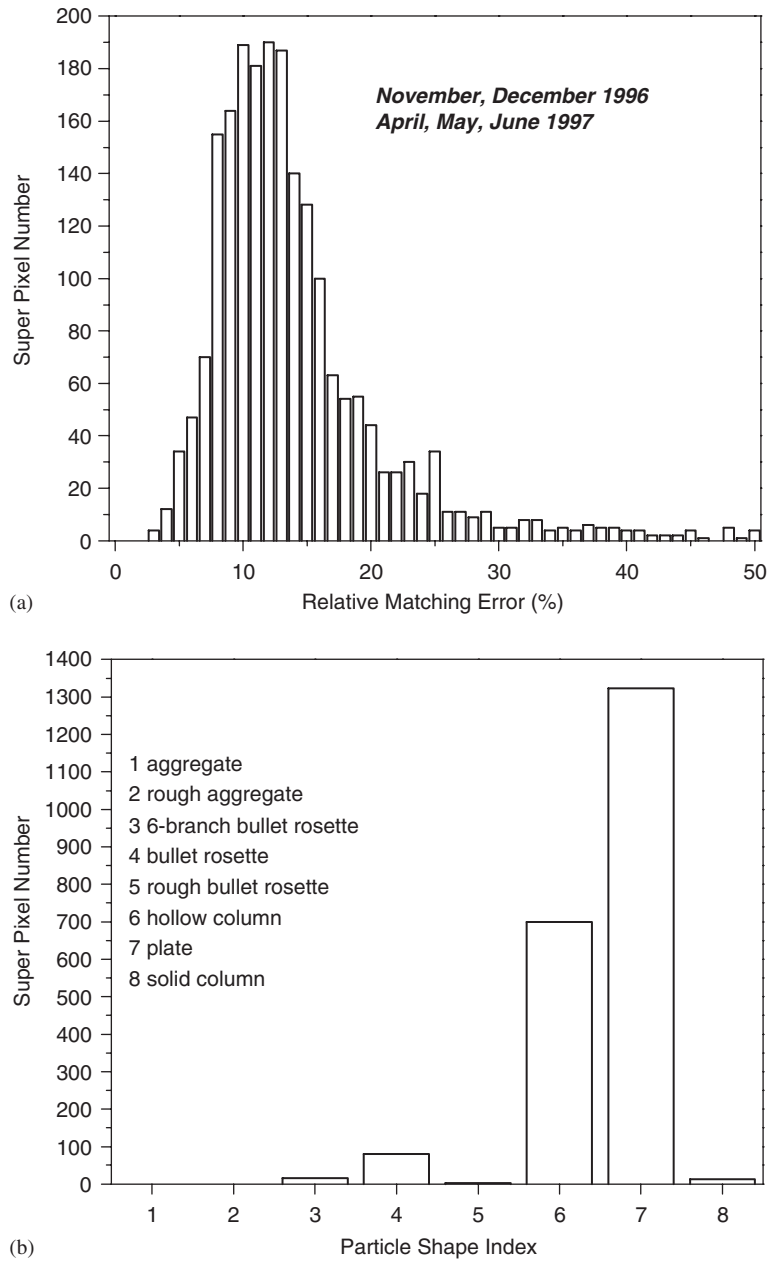


Fig. 7. (a) Relative matching error (RME) distribution for the 5-month POLDER data measured in November and December 1996, and April, May, and June 1997 for a latitude range of 60°S to 60°N and solar zenith angles smaller than 75°. (b) Super-pixel numbers as function of the particle shapes retrieved from the 5-month POLDER data. Among the 5-month POLDER data, only 2477 super-pixels satisfy the pixel selection criteria and are processed.

the theoretical plane-parallel cloud composed of randomly oriented ice crystals with single particle shape. Factors causing larger RME may include cloud top morphology, particle shape and size distributions [2], and the particle orientation [17]. Although the randomly oriented particle criteria are applied, the exclusion of preferably oriented particles is not warranted: the criteria to identify cloud pixels of randomly oriented particles are necessary but they might not be sufficient. Moreover, particle surface roughness [18,19] and particle inhomogeneity [20,21] can significantly reduce the polarization of the scattered light; they are also

factors which can affect the RME. Additionally, although POLDER's accuracy of the normalized polarized radiance is stated as being 0.001, the precision is not necessarily as good as this. The technical errors of the instruments may also be a cause of large RME values.

Fig. 7(b) shows the super-pixel numbers as function of the particle shapes retrieved from the 5-month POLDER polarized measurements. It shows that plates, hollow hexagonal columns, and bullet rosettes dominate the retrieved particle shapes. The number of super-pixels with retrieved solid hexagonal columns is very limited. However, this does not mean that solid hexagonal columns are not popular in ice clouds. One explanation is that hexagonal columns in ice clouds generally are not randomly oriented and the pixels dominated by them may have been excluded by the pixel selection criteria. On the other hand, based on the results from the sensitivity studies, we have to say that ambiguities may be unavoidable in the retrieved particle shapes due to the complicated particle shape mixture and particle orientations in actual ice clouds. When solid hexagonal columns are mixed with other particles of various shapes, their specific angular scattering features are "contaminated" by those of other particles. Therefore, the retrieved particle shape of the mixture can hardly be represented by the strongly featured hexagonal columns. Note here that the vertical inhomogeneity of cloud particle size and shape [22] can also affect the particle shape retrieval. Because the polarized radiance saturates at an optical thickness of 4, the retrieved particle shapes with the polarized radiance in this study may only represent those in the upper parts of the clouds.

5. Conclusions

In this study, a technique that applies single ice crystal habit and multidirectional polarized radiance to retrieve ice cloud particle shapes is evaluated. Using a database of theoretical TOA polarized reflectance at 865 nm for various combinations of particle shapes and size distributions, the MPRM method searches the database to find the cloud model that provides the best match to multi-angle POLDER polarized data over each super-pixel. In making the database of theoretical TOA polarized reflectance, we employ eight particle shapes and 30 ice crystal size distributions based on in situ observations. Our sensitivity studies show that the retrieved particle shapes from this algorithm can be considered good approximations to those in actual clouds in calculation of the phase matrix elements. However, this algorithm can only work well under the following conditions: (1) the retrievable must be overcast and thick ice cloud pixels, (2) the particles in the cloud must be randomly oriented, (3) the particle shapes and size distributions used in the lookup tables must be representative, and (4) the multi-angle polarized measurements must be accurate and sufficient to identify ice cloud pixels of randomly oriented particles. In practice, these conditions will exclude most of the measured cloud pixels. Additionally, because the polarized measurements are only sensitive to the upper cloud part not deeper than an optical thickness of 4, the retrieved particle shapes with the polarized radiance may only approximate those in the upper parts of the clouds. In other words, for thicker clouds with vertical inhomogeneity in particle shapes, these retrieved particle shapes cannot represent those of whole clouds. More robust algorithm is needed in accurate retrieval of ice cloud particle shapes.

Acknowledgments

The authors thank H. Chepfer for useful discussions and thank J.C. Buriez and F.M. Breon for their help on using POLDER polarized data. This study is supported by NASA grants NAG-1-2318 and NAG-1-01096.

References

- [1] Lynch DK, Sassen K, Starr DOS, Stephens G. *Cirrus*. New York: Oxford University Press; 2002.
- [2] Heymsfield AJ, Lewis S, Bansemer A, Iaquinta J, Miloshevich LM, Kajikawa M, et al. *J Atmos Sci* 2002;59:3–29.
- [3] Chepfer H, Minnis P, Young D, Nguyen L, Arduini RF. *J Geophys Res* 2002;107.
- [4] Deschamps PF, Breon FM, Leroy M, Podaire A, Bricaud A, Buriez JC, et al. *IEEE Trans Geosci Remote Sens* 1994;32:598–615.
- [5] Chepfer H, Goloub P, De Haan JF, Hovenier JW, Flamant PH. *J Geophys Res* 2001;106:7955–66.
- [6] Masuda K, Ishimoto H, Takashima T. *J Quant Spectrosc Radiat Transfer* 2002;75:39–51.
- [7] Buriez JC, Vanbauce C, Parol F, Goloub P, Herman M, Bonnel B, et al. *Int J Remote Sens* 1997;18:2785–813.

- [8] Parol F, Buriez JC, Vanbauce C, Couvert P, Seze G, Goloub P, et al. *IEEE Trans Geosci Remote Sens* 1999;37:1597–612.
- [9] Goloub P, Herman M, Chepfer H, Riedi J, Brogniez G, Couvert P, et al. *J Geophys Res* 2000;105:14,747–59.
- [10] Yang P, Liou KN, Wyser K, Mitchell D. *J Geophys Res* 2000;105:4699–718.
- [11] Fu Q. *J Climate* 1996;9:2058–82.
- [12] Mitchell DL, Chai SK, Liu Y, Heymsfield AJ, Dong Y. *J Atmos Sci* 1996;53:2952–66.
- [13] Evans KF, Stephens GL. *J Quant Spectrosc Radiat Transfer* 1991;46:413–23.
- [14] Heymsfield AJ, Platt CMR. *J Atmos Sci* 1984;41:846–56.
- [15] Baum BA, Kratz DP, Yang P, Ou SC, Hu Y, Soulen PF, et al. *J Geophys Res* 2000;105:11,767–80.
- [16] King MD, Platnick S, Yang P, Arnold GT, Gray MA, Riedi JC, et al. *J Atmos Ocean Technol* 2004;21:857–75.
- [17] Chepfer H, Brogniez G, Goloub P, Breon FM, Flamant PH. *J Quant Spectrosc Radiat Transfer* 1999;63:521–43.
- [18] Sun W, Loeb NG, Videen G, Fu Q. *Appl Opt* 2004;43:1957–64.
- [19] Li CH, Kattawar GW, Yang P. *J Quant Spectrosc Radiat Transfer* 2004;89:123–31.
- [20] Labonnote LC, Brogniez G, Doutriaux-Boucher M, Buriez JC. *Geophys Res Lett* 2000;27:113–6.
- [21] Labonnote LC, Brogniez G, Buriez JC, Doutriaux-Boucher M, Gayet JF, Macke A. *J Geophys Res* 2001;106:12139–53.
- [22] Heymsfield AJ, Iaquinta J. *J Atmos Sci* 2000;57:916–38.